ELSEVIER

Physica B 252 (1998) 34–43

PHYSICA B

Coherence volumes and neutron scattering

J. Felber[a,*], R. Gähler[a], R. Golub[b], K. Prechtel[a]

[a] *Fakultät für Physik E21, Technische Universität München, D 85747 Garching, Germany*
[b] *Hahn Meitner Institut, Glienicker Str. 100, D 14109 Berlin, Germany*

Received 29 October 1997; accepted 19 December 1997

Abstract

We describe neutron scattering in a space–time frame-complementary to the van Hove picture. Based on the theory of partial coherence from light optics, neutron beams may be represented by correlation volumes, which are defined by the wavelength distribution and by optical elements like guides, slits, choppers or crystals. Size and shape of these tiny volumes (in space and time) determine the volume of coherent interaction within the samples, which are represented by pair correlation functions. The beam correlation volumes also determine the resolution of the experiment and if the signal is proportional to a Fourier transform of the sample correlation function. Here we give a simple approach to this theory with various examples.

Keywords: Neutron scattering; Partial coherence; Cittert–Zernike theorem

1. Introduction

Scattering of neutrons from condensed matter is commonly described by the van Hove formalism [1]. For an incoming plane wave the scattering process is formulated in terms of momentum and energy transfer, q and ω. Instrumental effects on resolution are included afterwards by averaging the scattered intensities for a certain range of in- and outgoing wavevectors.

An alternative approach to neutron scattering was given recently [2]. This approach, presented here in a simple picture, shows a closer link between the scattering process and the instrument, as the scattering is calculated directly for the wave field shaped by the spectrometer. On the scale of a typical sample size, the surfaces of constant phase are far from being planar. This condition which only holds within tiny volumes, normally not exceeding the nm scale. We characterize these fields by using the theory of partial coherence from light optics [3]. For each point P_0 within the wave field, this theory derives a certain volume V_c around P_0, with a well defined phase w.r.t. the phase at P_0. V_c can be considered as coherence or correlation volume,[1] with fairly a plane wave inside but more or less random phase relations outside of this volume. Because of this randomness, scattering experiments with neutrons (or other particles) reveal knowledge on correlations between atoms only within the scale of V_c, and the correlation lengths which define V_c determine the resolution of the experiment.

* Corresponding author.

[1] Subtle differences between coherence and correlation are not taken into account and we use both expressions as equivalent.

0921-4526/98/$ – see front matter
PII: S0921-4526(97)00999-X

We will first derive correlation lengths for two basic cases and then estimate V_c for several devices commonly used in neutron scattering. Then we apply these volumes for several scattering experiments, where we describe the samples by pair correlation functions $G(r, t)$. The shape and size of V_c also determine, whether $G(r, t)$ itself or its Fourier transforms w.r.t. r and/or t are measured in the experiment.

2. The van Cittert–Zernike theorem in space and time

Similar to light emitted by thermal sources, neutron beams emerging from moderators of reactors may be considered as completely incoherent, i.e. with random phase variations for radiation coming from neighboring source points. But "… coherence is created by the very process of propagation" [4], and in some distance downstream from the source there exists a well defined phase relation within a certain volume, which gives rise to coherence in the sense of classical optics. An intuitive explanation of this phenomenon is shown in Fig. 1a.

A quantitative description of these coherence properties for light beams was first derived by van Cittert and Zernike (CZ-theorem) [5,6], which is shown in Fig. 1b. For stationary neutron beams (and elastic neutron scattering) their results are equally valid, as the wave equations (the Helmholtz equation for light and the stationary Schrödinger equation for massive particles) are of the same kind. For time-dependent optics (and inelastic scattering) both equations are different and thus we expect different coherence properties for light and massive particles.

Many textbooks, e.g. [3,7,8], derive the CZ-theorem for the stationary case; for a treatment of the time-dependent case see Ref. [9]. In the present discussion we will not use the full correlation function, but only the mean lengths associated with it.

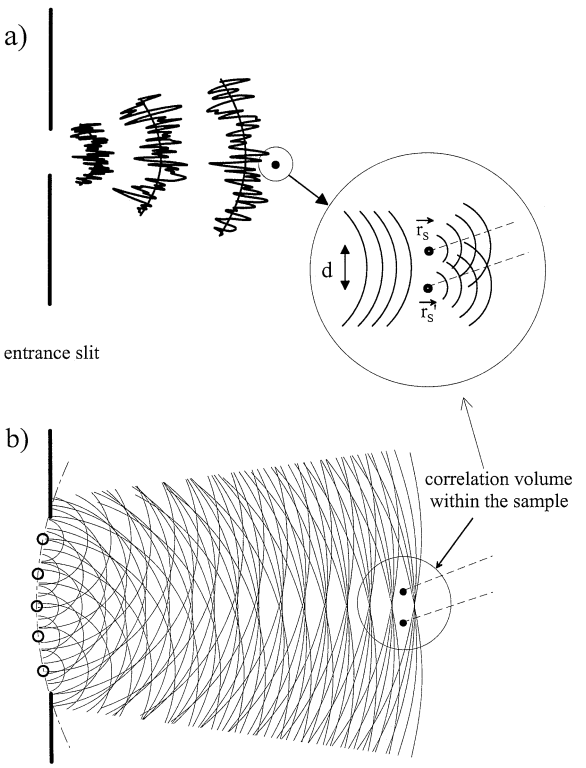

Fig. 1. Two different views of the wave field emerging from a completely incoherent source. (a) The wave field with its statistical fluctuations. These are small only on a length scale of d, where d increases with the distance from the source. (b) View of the van Cittert–Zernike theorem; the coherence function for an incoherent source (the entrance slit) is given by the amplitude of the diffraction pattern for spherical incoming waves which focus at the point of observation. We apply Huygens' principle to show this diffraction pattern.

2.1. The CZ theorem in space – the correlation width of a slit

A slit of width $2a$ is illuminated from the left by an incoherent source, e.g. a neutron moderator. There are no phase correlations between waves emerging from neighboring points in the slit. According to Huygens' principle, each of these points is a source of outgoing spherical waves $\Psi(r)$, given by

$$\Psi(r) = \frac{e^{ikr + \varphi_0}}{r}, \tag{2.1}$$

where k denotes the wave vector, r the distance from the source point and φ_0 is the randomly varying phase. At a screen A in a distance L downstream of the slit (see Fig. 2), we determine the lateral width of coherence x_c in the following

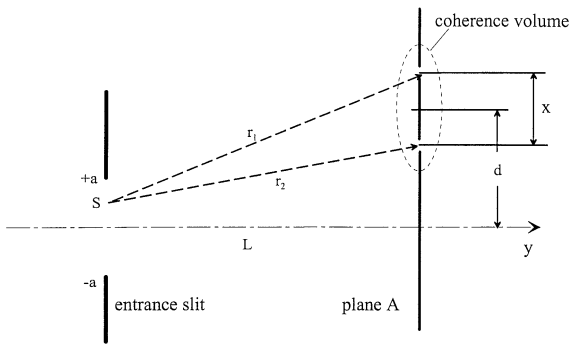

Fig. 2. Correlation length x_c for a single slit. Spherical waves emerging from a source point S in the entrance slit pass through two pin holes separated by x in plane A and will give rise to a double-slit pattern (not shown) downstream of this plane. For all different source points, $r_1 - r_2$ should not vary by more than about $\lambda/2\pi$, in order to maintain high contrast of the double slit pattern. For given a, L and wavelength λ, this defines a maximum separation x_c – the correlation length, which to first-order is independent of d. The resulting coherence or correlation volume is indicated.

gedanken experiment (see Ref. [6]): we assume two pinholes separated by x in the screen and determine as a function of x the contrast of the double-slit pattern of the waves passing these slits.

This loss in contrast results from the fact that at both holes the phase difference $k(r_1 - r_2)$ of the waves emerging from one source point S in the entrance slit will vary with the position of S within the slit. As we calculate the intensities of the pattern separately for each source point, it is only this variation but not the phase φ_0 which reduces the contrast. Based on this, we can give a simple first-order estimate of x_c. For waves emerging from the center of the entrance slit the path difference ΔL_0 at the two pin holes, centered around d will be, assuming $x_c \ll d$

$$\Delta L_0 = \frac{d}{L} x_c; \qquad \Delta\varphi_0 = k\Delta L_0. \tag{2.2}$$

For waves emerging from one of the edges of the slit, the corresponding path difference $\Delta L_{\pm a}$ will be:

$$\Delta L_{\pm a} = \frac{d \pm a}{L} x_c. \tag{2.3}$$

The variation $\Delta L = |\Delta L_{\pm a} - \Delta L_0|$ of both path differences, which causes the loss of contrast, is independent of d,

$$\Delta L = \frac{a}{L} x_c. \tag{2.4}$$

For a mean phase variation of $\Delta\varphi = 1$ with $\Delta\varphi = k\Delta L$ we get

$$x_c = \frac{L}{ka}. \tag{2.5}$$

In a more rigorous treatment [3,6,9], the coherence function γ is used, where

$$\gamma = \frac{\sin u}{u}, \qquad u = \frac{ka}{L} x. \tag{2.6}$$

For $u = 1$ the degree of coherence drops from 1 (for $x = 0$) to 0.84, which gives the coherence length Eq. (2.5). Within this range of x_c the phase differences for all waves at the screen A are fairly constant, leading to high contrast of the double-slit pattern. Note again that in this calculation the arbitrary phase φ_0 of the waves within the source area does not play a role for the contrast, and we see that the wave field emerging from an incoherent source acquires some coherence by traveling. In z direction (the direction of traveling), for stationary beams, the longitudinal coherence is given by $\lambda^2/\Delta\lambda$.

2.2. *The CZ-theorem in time – the correlation time for a chopped beam*

Consider now a chopper of opening time $2T$ is illuminated from the left with a white spectrum of neutrons. We take the chopper opening as a square function in time with a wide open area in order to make diffraction in space negligible. Within this time window of $2T$ we assume no phase correlations between waves passing the chopper at different times. Nevertheless there will be phase correlations within certain correlation times t_c downstream of the chopper, which – at least in a gedanken experiment – can be measured with a Michelson interferometer.

The estimate of t_c will be similar to the one for x_c in the spatial case. We assume $t_c \ll 2T \ll t_0$ with t_0 being the classical flight time for a particle of matter wave frequency ω_0 from the chopper to the plane of observation A in distance L from the chopper (see Fig. 3a). Two waves emerging from the chopper at time $t = 0$ will have a certain phase difference $\Delta\varphi_0$ in plane A, if we consider two different flight times $t_0 \pm t_c/2$:

$$\Delta\varphi_0 = \varphi(t_0 - t_c/2) - \varphi(t_0 + t_c/2). \tag{2.7}$$

As we deal with time-dependent effects in this case, we will use the Green's function of the time dependent Schrödinger equation, which is given by [10,11]

$$\Psi = \exp\left[\mathrm{i}\frac{mL^2}{2\hbar\tau}\right], \tag{2.8}$$

where τ is the flight time. We obtain for the phase difference at the two times separated by t_c

$$\Delta\varphi_0 = \frac{mL^2}{2\hbar}\left(\frac{1}{t_0 - t_c/2} - \frac{1}{t_0 + t_c/2}\right) \approx \frac{mL^2 t_c}{2\hbar t_0^2} = \omega_0 t_c \tag{2.9}$$

with ω_0 being the mean matter-wave frequency. For waves emerging from the chopper at opening time $\pm T$, we get for the phase difference $\Delta\varphi_{\pm T}$ for the same arrival times as before:

$$\Delta\varphi_{\pm T} = (\omega_0 \mp \Delta\omega)t_c, \qquad \frac{\Delta\omega}{\omega_0} = \frac{2T}{t_0}, \tag{2.10}$$

where $\Delta\omega$ is the change in matter-wave frequency to account for the mean change in flight time from t_0 to $t_0 \mp T$. The two phase differences $\Delta\varphi_{\pm T}$ and $\Delta\varphi_0$ should not be different by more than $\simeq 1$, which is the analog coherence condition to the spatial case, and which determines t_c. It follows:

$$|\Delta\varphi_{\pm T} - \Delta\varphi_0| = 1 = \Delta\omega t_c = \frac{2T\omega_0}{t_0} t_c\,, \tag{2.11}$$

$$t_c = \frac{t_0}{\omega_0 2T}\,. \tag{2.12}$$

Within time elements of t_c the waves in plane A can be taken as coherent (see Fig. 3b). Note that t_c is proportional to the mean travel time, whereas for continuous beams the correlation time t_c [3] is constant:

$$t_c = \lambda^2/(\Delta\lambda v)\,,$$

Time-dependent slits are often made by two counter rotating choppers close together. For identical

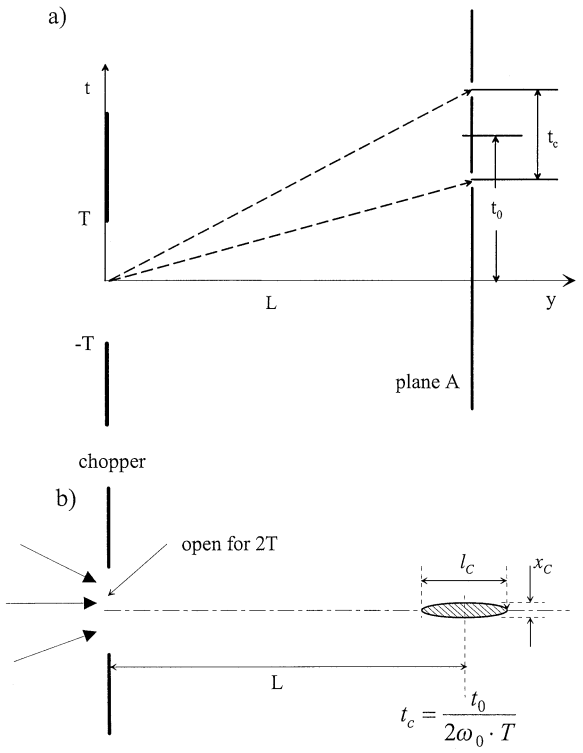

Fig. 3. Correlation time for a chopper. (a) Spherical waves emerging at a certain time within the chopper opening pass through two 'pin holes in time' separated by t_c in plane A and will give rise to a double-slit pattern in time (not shown) downstream of this plane. For all waves, passing the chopper during the opening time $2T$, the phase differences at the two 'pin holes' should not vary by more than about 1, in order to maintain high contrast of the double-slit pattern. This defines a maximum separation time t_c – the correlation time – for given T, mean flight time t_0 and mean matter-wave frequency ω_0. (b) For standard neutron spectrometers, t_c is orders of magnitudes smaller than the chopper opening time. The correlation length x_c perpendicular to the beam is determined by the slit width of the chopper.

slit widths and velocities the opening function is of triangular shape. For a time width $2T$ (FWHM), we obtain as correlation time

$$t_c = 0.72 \frac{t_0}{2\omega_0 T}. \tag{2.13}$$

3. Correlation volumes for further neutron optical devices

3.1. Monochromating crystal

Bragg scattering from crystals with fairly small mosaicity, as often used in triple axis spectrometers [12], gives a dominant correlation length l_g in direction of the reciprocal lattice vector $\boldsymbol{G}$ (see Fig. 4), whereas the situation may be quite different for large mosaicities or for gradient crystals [13]. As the momentum space volume V_p and the correlation volume V_c are conjugate volumes ($V_p V_c \approx \hbar^3$) [9], the shape of V_c can always be deduced from the known shape of V_p, which is strongly dependent on the crystal properties.

We estimate the length of l_g by the typical size s of a crystallite, as we get coherent superposition of scattered waves only within s, which is assumed to be smaller than the primary extinction length [14]. The correlation length $l_\perp$ perpendicular to l_G is determined by the mosaicity $\Delta\Theta$ of the crystal and the beam divergence, and as stated above, we assume $l_\perp$ significantly smaller than l_g.

It follows that the correlation volume in the case of Bragg scattering is tilted by the Bragg angle Θ w.r.t. the beam axis, an effect of particular importance for phonon focussing, as will be shown below. Note that in our simple picture the length of V_c does not depend on the neutron velocity, but is just a crystal property.

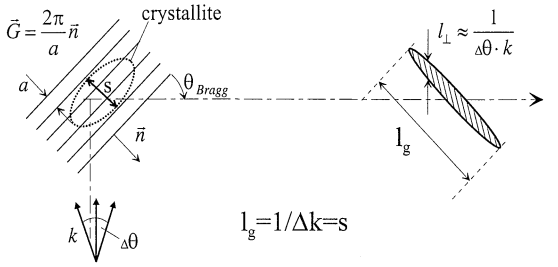

Fig. 4. For Bragg reflection from a crystal with small mosaicity, the correlation length can be estimated as the typical size of a crystallite. The correlation volume is tilt w.r.t. the beam axis.

3.2. Magnetic field

Neutrons of energy E_0 may have two states of different energies $E_0 \pm \mu B$ in a magnetic field of strength B, with μ being the neutron magnetic moment. After passage through a field of length L, tilted by an angle θ w.r.t. the beam axis (see Fig. 5), the correlation volumes of the two states are separated by $\boldsymbol{\delta}_B$ where the unit vector $\boldsymbol{n}$ is normal to the field boundary.

$$\boldsymbol{\delta}_B = \frac{2\mu B}{mv^2} \frac{L}{\cos\Theta} \cdot \boldsymbol{n}. \tag{3.1}$$

It may be noted that this separation occurs without change in the shape of the incoming correlation volume. In spin echo spectrometry, $\boldsymbol{\delta}_B/v$ is called spin echo time. In these instruments, after the scattering process both states get recombined again by a second magnetic field and the polarization is determined from adding the amplitudes of both states.

3.3. Detector

We assume a detector with pointlike absorbers randomly distributed behind the exit slit. As there

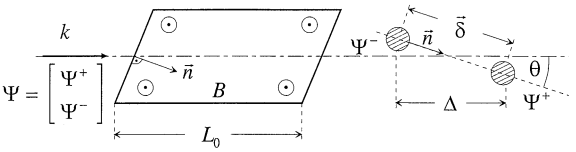

Fig. 5. The different energies of the two eigenstates of a neutron in a magnetic field lead to a separation of their correlation volumes. For parallel field boundaries, the separation is in the direction of the normal to these boundaries. The longitudinal separation Δ expressed as a time delay, is the well known spin echo time τ.

are no interference effects between different absorption processes, we may describe the wave field by incoming spherical waves centered at the absorbers, and the situation is somewhat similar to the source slit, where we assumed independent outgoing spherical waves. Consequently, we may define a correlation volume at the sample due to the detector, which we denote as backward correlation volume V_{cb}. This means that paths going through pairs of scattering points whose separation lies outside the 'back correlation' volume, lose correlation on travelling from the scattering points to a single absorbing point in the detector. For an exit slit of width $2d$ we get as backward correlation length:

$$x_{cb} = \frac{L_d}{kd}, \tag{3.2}$$

where L_d is the distance from the sample to the detector.

In case of a detector with time resolution $2T_d$ the backward correlation time at the sample is given by

$$t_{cb} = \frac{t_d}{2\omega T_d}, \tag{3.3}$$

where t_d is the flight time and ω is the mean matter-wave frequency of particles arriving at the detector within time elements $2T_d$.

4. Description of various instruments

In the following we consider for various simplified cases the interaction of the sample with the wave fields inside these correlation volumes. This sample may be fully described by its density of scatterers $\rho(r)$ or $\rho(r, t)$ in case of a time-dependent system. We assume the same scattering length for all atoms, a generalization to different ones would be straightforward.

4.1. Small-angle scattering (SANS)

A simple SANS device consists of two slits S_1, S_2 separated by a distance L_1, with the sample close to S_2 and a detector with a certain spatial resolution $2d$ downstream of S_2 at a distance L_2.

The lateral correlation length x_c at the sample due to slit S_1 of width $2a$ is given by

$$x_c = \frac{L_1}{k_1 a}. \tag{4.1}$$

According to Section 2, the dominant extension of V_c is in x-direction and we will assume that phase variations of waves scattered within V_c only depend on x. We also assume that the density of scatterers is only a function of x, i.e. $\rho = \rho(x)$. The amplitude emerging from a scatterer at x inside V_c is proportional to $\rho(x)$. The intensity at the detector due to all scattered waves from V_c will be proportional to the sum of all cross products of $\rho(x)$ and $\rho(x + \delta)$, where δ varies within the range of x_c. For a small scattering angle $\varphi = q/k_1$, the phase difference $\Delta\varphi$ between waves scattered from x and $x + \delta$ (see Fig. 6) will be

$$\Delta\varphi = (\boldsymbol{k}_1 - \boldsymbol{k}_2)\cdot\boldsymbol{\delta} = \boldsymbol{q}\cdot\boldsymbol{\delta} \approx q\delta, \tag{4.2}$$

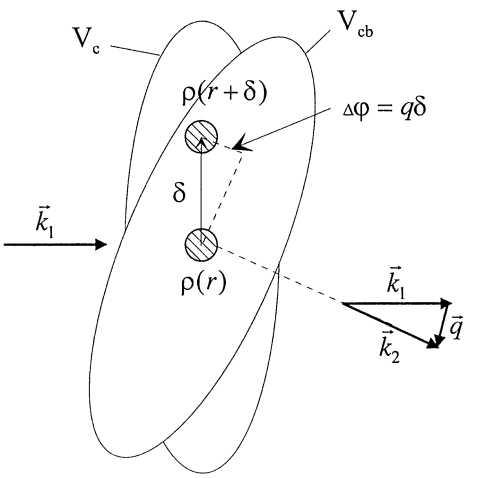

Fig. 6. In small-angle neutron scattering, the incoming correlation volume V_c has its main extension x_c perpendicular to k_1. This allows to measure sample correlations with $\delta \gtrsim x_c$, which may reach values up to μm in SANS instruments. Adding of all products of scattered waves from $\rho(r)$ and $\rho(r + \delta)$ leads to the Fourier transform of $G(r, t)$. The resolution is limited to the intersection volume of the in- and outgoing correlation volume V_c', which shows the relation between monochromaticity and scattering angle.

where q is the momentum transfer, k_1 and k_2 ae the in- and outgoing wave vectors. The phase $\Delta\varphi$ may also be seen from the outgoing volume V_{cb}, where a plane wavefront in the direction of $\boldsymbol{k}_2$ implies an appropriate correlation length in the sample.

Well defined phase relations within the outgoing wave field can only exist within the intersection volume $\bar{V}_c = V_c \cap V_{cb}$, which has a length of $\overline{x_c}$. This shows the close-link between wavelength band and q-resolution. With increasing q the beam monochromaticity has to be enhanced, to maintain significant overlap (length of $\overline{x_c}$) between V_c and V_{cb}. As intensity we get from summing over all scattered waves within $\overline{x_c}$:

$$I = c\int_{\overline{x_c}} \rho(x)\rho(x+\delta)e^{-iq\delta}\,d\delta = \int_{\overline{x_c}} G(\delta)e^{-iq\delta}\,d\delta, \quad (4.3)$$

where $G(\delta)$ is the pair correlation function within the correlation volume $\bar{V}_c$. Enlargement of the sample above $\bar{V}_c$ does not yield new information, except for better statistics. Averaging over all correlation volumes (i.e. over all positions x) within the sample leads to

$$I_{tot} = c\int_{sample} G(\delta)e^{-iq\delta}\,d\delta. \quad (4.4)$$

Correlations up to the lateral correlation width $\overline{x_c}$ will be visible and in this sense, $\overline{x_c}$ can be considered as the spatial resolution of the experiment. If significant correlations within the sample are limited to distances $\delta < \overline{x_c}$, then Eq. (4.4) is the Fourier transform of $G(\delta)$.

The maximum lateral width $2b$ of the sample can be estimated from Fig. 7. We consider a correlation volume centered around b instead of being on the optical axis, which leads to some dephasing of the waves at the detector. As before we may tolerate a maximum path difference

$$(l_1' + l_2') - (l_1 + l_2) = \lambda/2\pi = 1/k. \quad (4.5)$$

Assuming $x_c \ll b \ll L_1, L_2$ we get

$$b \approx \frac{1}{kx_c}\left(\frac{L_1 L_2}{L_1 + L_2}\right). \quad (4.6)$$

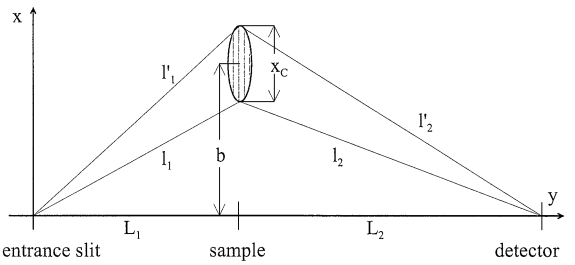

Fig. 7. Estimate of the maximum sample size (width $2b$; $x_c \ll b$) in SANS. Shifting the correlation volume off the axis by a length b, leads to a path difference $l_1' + l_2' - (l_1 + l_2)$, which should not exceed $\lambda/2\pi$.

The above consideration may be compared with Eq. (18) in Ref. [2]: The three $\sin u/u$ factors fall significantly, if δ exceeds x_c and consequently the main contribution to the integral comes from values $\delta \gtrsim x_c$, i.e. from inside the correlation volume. For intensity reasons, the arguments of all the $\sin u/u$ functions should be made equal, which leads to:

$$b\left(\frac{1}{L_1} + \frac{1}{L_2}\right) = \frac{d}{L_2} = \frac{a}{L_1}, \quad (4.7)$$

which may also be obtained from the present consideration.

4.2. Time of flight spectrometer (TOF)

The time equivalent of a SANS instrument consists of two choppers Ch_a and Ch_S, with the sample close to Ch_S and a detector D with a certain time resolution. The correlation time t_c at the sample due to the chopper Ch_a with opening time $2T_a$ is

$$t_c = \frac{t_1}{2\omega_1 T_a}, \quad (4.8)$$

where ω_1 is the mean matter wave frequency and t_1 is the mean time of flight between Ch_a and Ch_S. In analogy to scattering in space, only sample correlation times which are not much greater than t_c will be observable in the experiment. This also

holds for the 'backward' correlation time

$$t_{cb} = \frac{t_2}{2\omega_2 T_D} \tag{4.9}$$

seen from the detector at the sample where t_2 is the mean time of flight between Ch_S and D, with $2T_D$ being the time resolution of the detector (see Fig. 8). Again, t_c should be matched to t_{cb} because of intensity reasons.

The total amplitude is obtained from integrating all scattered amplitudes within the correlation time t_c. In calculating the intensity via all cross products of $\rho(r, t)$ and $\rho(r, t + \tau)$ we get an additional phase factor in the integrand. In analogy to the SANS case (correlating two scattered waves separated in space), this leads to a Fourier transform, but now w.r.t. time: The correlation of two waves scattered with a time delay τ leads to a phase difference (see Fig. 8)

$$\Delta\varphi = \omega_1\tau - \omega_2\tau = \omega\tau. \tag{4.10}$$

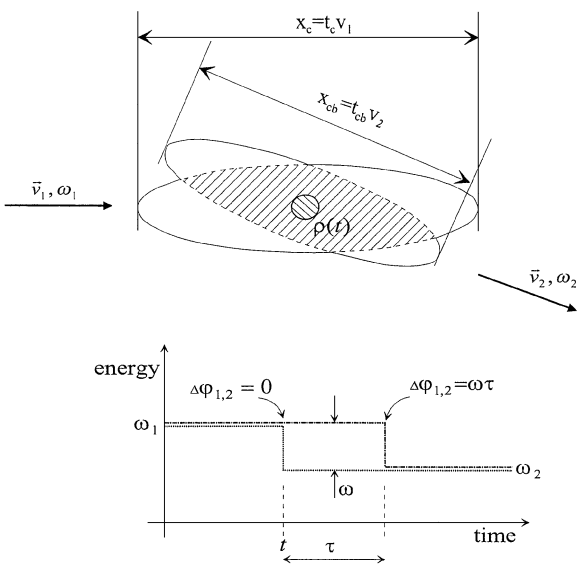

Fig. 8. Quasielastic scattering. The correlation volumes exhibit maximum extensions parallel to k, and allow for a long interaction time with a localized excitation given by $\rho(t)$. Integration over the interaction time leads to the Fourier transform of $G(r, t)$ w.r.t. time.

For the scattered intensity we get

$$I \propto \int_{t_c} S(q, \tau)\, e^{-i\omega\tau}\, d\tau, \tag{4.11}$$

where we assumed a certain momentum transfer q similar to the SANS case. If all significant time correlations in the sample are smaller than t_c, Eq. (4.11) is the Fourier transform of $S(q, t)$. Accessible time correlations are limited to t_c, and hence t_c can be considered as time resolution of the instrument.

The maximum opening time $2T_S$ of the chopper Ch_S may be estimated analog to the sample size in the spatial case:

We consider correlations in time centered around a time t_1' (instead of t_1) with $t_1' = t_1 + T_S$ and may tolerate an additional phase difference of 1. From Eq. (2.8), using $t_c \ll T_S \ll t_1,\ t_2$, we finally obtain:

$$T_S \simeq \frac{\hbar/(mt_c)}{v_1^3/L_1 + v_2^3/L_2}, \tag{4.12}$$

where v_1 and v_2 are the mean velocities before and after scattering.

For $L_1 = L_2$ and $v_1 \approx v_2 = v$ we get

$$T_S \simeq \frac{t}{2kvt_c}, \tag{4.13}$$

where t is the mean flight time. Eq. (4.13) is closely related to Eq. (4.6), which estimates the sample width in the SANS case, assuming $L_1 = L_2 = L$.

Eq. (4.13) may be compared with Eq. (48) from Ref. [2], which contains correlation functions for both arms of the spectrometer and the sample. For intensity maximizing reasons, these three factors should be made equal, and we get:

$$k_1^2 T = k_2^2 T_D = 2(k_1^2 + k_2^2) T_S. \tag{4.14}$$

4.3. Triple-axis spectrometer

Triple-axis instruments are commonly used to determine nonlocalized excitations e.g. phonons in crystals, and these spectrometers cover a large range in momentum transfer q and energy transfer

ω. Here, special emphasis is given to measurements of life times of those excitations, which gives information on electron phonon coupling and on unharmonicities of the lattice.

With respect to size and shape of V_c, we assume the monochromating and analyzing crystals to be the dominant optical elements of triple-axis instruments (see Section 3). As we deal with time-dependent phenomena, we have to take into account the time dependence of both correlation volumes during the scattering process, i.e. the movement of V_c with the neutron velocity. This is similar to the TOF case, whereas in the SANS case, V_c could be taken as static.

In analogy to the above cases, significant contributions to the total amplitude at the detector may only come from the overlap volume $\bar{V}_c = V_{c1} \cap V_{c2}$, where the indices 1 and 2 denote the monochromator and analyzer crystal. Due to the tilt of both volumes w.r.t. their beam axes, $\bar{V}_c$ moves with a certain velocity $\boldsymbol{v}_c$ (see Fig. 9). By matching $\boldsymbol{v}_c$ to the velocity $\boldsymbol{v}_p$ of a moving excitation, i.e. to a phonon, we obtain a fairly long interaction time. The relation between the relevant vectors for this 'phonon focusing' condition may be deduced from

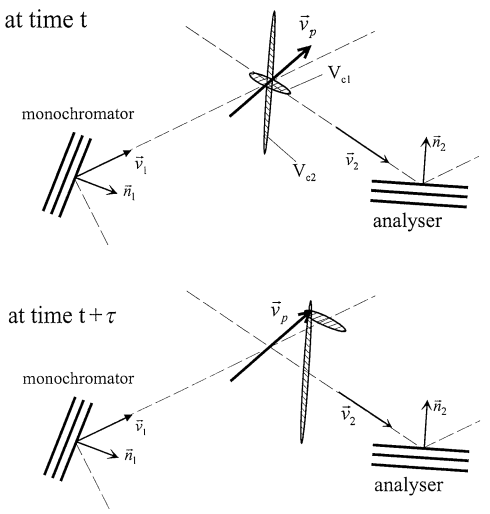

Fig. 9. Triple-axis spectrometer in focusing geometry. The intersection of the coherence volumes V_{c1} and V_{c2} moves with the phonon, represented by v_p. Phonon lifetimes smaller than the interaction time can be observed. The focusing conditions may be deduced directly from the figure.

Fig. 10:

$$\boldsymbol{n}_1 \cdot l_{g1} = (\boldsymbol{v}_1 - \boldsymbol{v}_p)\tau, \quad \boldsymbol{n}_2 \cdot l_{g2} = (\boldsymbol{v}_p - \boldsymbol{v}_2)\tau, \tag{4.15}$$

where $l_{g1/2}$ are the lengths of the correlation volumes of the monochromator and analyzer and τ is the relevant correlation time for the interaction. In a space-time picture, (see Ref. [15]) this excitation can be described by a specific correlation function G:

$$G(\boldsymbol{R}, \tau) = \mathrm{e}^{-\Gamma \cdot \tau} \cdot \delta^{(3)}(\boldsymbol{R} - \boldsymbol{v}_p \cdot \tau), \tag{4.16}$$

where Γ is the life time of the excitation, being located in space around $\boldsymbol{R}$. In order to measure Γ, the interaction time τ, i.e. the time of overlap between R and $\bar{V}_c$, should not be less than about $1/\Gamma$, and together with Eq. (4.15) this condition determines minimum values of l_{g1} and l_{g2} for given $\boldsymbol{v}_1$ and $\boldsymbol{v}_2$. Using Eq. (4.15) we obtain:

$$\boldsymbol{n}_1 \cdot l_{g1} + \boldsymbol{n}_2 \cdot l_{g2} = (\boldsymbol{v}_1 - \boldsymbol{v}_2)\tau = c\boldsymbol{q} \tag{4.17}$$

where $\boldsymbol{q}$ is the momentum transfer and c is a constant, given by the interaction time τ and by momentum conservation in the scattering process. Eq. (4.17) is the triple-axis focusing condition in the space–time picture. For the focusing condition in the q–ω picture, we refer to Refs. [16,17]. Energy conservation in the scattering process sets an additional constraint to the possible values of $\boldsymbol{v}_1$ and $\boldsymbol{v}_2$.

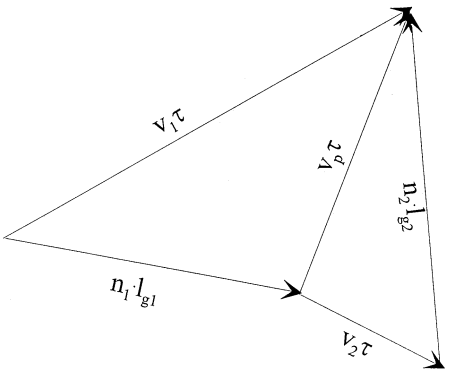

Fig. 10. Relation between the n-velocities v_1/v_2, the phonon velocity v_p, the correlation lengths l_{g1} and l_{g2} for the in- and outgoing beams and the interaction time τ.

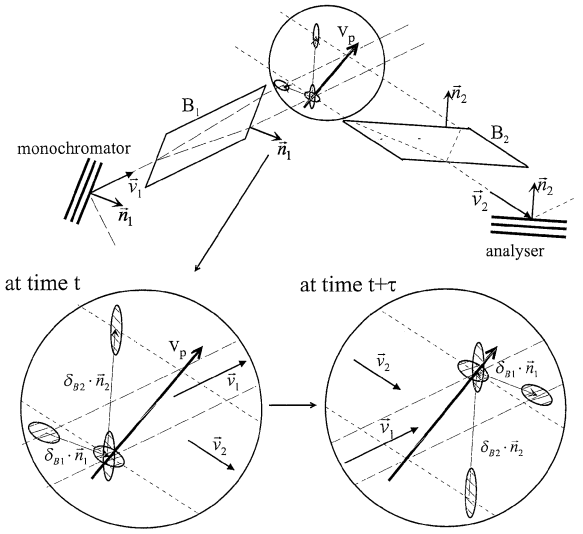

Fig. 11. Triple-axis spectrometer with spin-echo fields in focusing geometry. We assume that the correlation lengths due to the crystals are much smaller than the splittings due to the *B*-fields. The focusing condition is similar to the pure triple axis case. By varying the magnitude and the direction of the field boundaries of the *B*-fields, the focusing condition can be matched to a wide range of phonon parameters.

4.4. Triple-axis spectrometer with spin echo option

We now place magnetic precession fields B_1 and B_2 upstream and downstream of the scattering sample (see Fig. 11) and assume the boundaries of each field to be tiltable w.r.t. the beam axis by angles Θ_1 and Θ_2. We further assume that all dimensions of the correlation volumes $V_{c1,2}$ are small compared to the splittings caused by the *B*-fields, i.e. we assume $l_g \ll |\boldsymbol{\delta}_B|$ (see Eq. (3.1)). The focusing condition, which was first derived in Ref. [18] is similar to the pure triple axis case, but the fixed lengths of $l_{g1,2}$ (given by the crystal properties) are replaced now by the splittings $\boldsymbol{\delta}_{B1,2}$. The condition for overlap of the corresponding correlation volumes for the in- and outgoing beam i.e. the focusing condition, which may be derived from Fig. 11, reads:

$$\boldsymbol{n}_1 \| \boldsymbol{v}_1 - \boldsymbol{v}_p, \quad \boldsymbol{n}_2 \| - \boldsymbol{v}_2 + \boldsymbol{v}_p. \tag{4.18}$$

The magnitude as well as the direction of $\boldsymbol{\delta}_B$ can be varied in a wide range by changing the magnitude and the shape of the *B*-fields. The focusing conditions (4.18) can now be fulfilled for a large range of experimental parameters, and the high energy resolution of spin echo can be combined with the wide space–time (or q–ω) range of triple-axis spectrometers. A spectrometer of this kind was built for the HMI Berlin [19].

References

[1] L. van Hove, Phys. Rev. 95 (1954) 249.
[2] R. Gähler, J. Felber, F. Mezei, R. Golub, Phys. Rev. A, submitted.
[3] M. Born, E. Wolf, Principles of Optics, 6th edn., Pergamon Press, Oxford, 1980.
[4] A.S. Marathay, Elements of Optical Coherence Theory, Wiley, 1982.
[5] P.H. van Cittert, Physica 1 (1934) 201.
[6] F. Zernike, Physica 5 (1938) 785.
[7] D. Champeney, Fourier Transforms and their Physical Applications, Academic Press, New York, 1973.
[8] J.Ph. Peres, Optik, Spektrum, Akad., Verlag, Heidelberg, 1996.
[9] T. Keller, W. Besenböck, J. Felber, R. Gähler, R. Golub, P. Hank, M. Köppe, Physica B 234–236 (1997) 1120.
[10] P.M. Morse, H. Feshbach, Methods of Theoretical Physics, vol. 1,7, McGraw-Hill, New York, 1953.
[11] R. Golub, R. Gähler, Z. Phys. B 56 (1984) 5.
[12] B. Dorner, Springer Tracts in Modern Physics, vol. 93, Springer, Berlin, 1982.
[13] A. Magerl, J. Neutron Res. 5 (1996) 41.
[14] H. Maier-Leibnitz, Nukleonik 8 (1966) 5.
[15] R. Gähler, R. Golub, K. Habicht, T. Keller, J. Felber, Physica B 229 (1996) 1.
[16] R. Stedman, Rev. Sci. Instr. 39 (1968) 878.
[17] M.J. Cooper, R. Nathans, Acta Crystallogr. 23 (1967) 357.
[18] F. Mezei (Ed.), Neutron Spin Echo, Lecture Notes in Physics, vol. 128, Springer, Berlin, 1980.
[19] T. Keller, R. Gähler, H. Kunze, R. Golub, Neutron News 6 (3) (1995) 16.